



Deligianni, F., Wong, C., Lo, B. and Yang, G.-Z. (2018) A fusion framework to estimate plantar ground force distributions and ankle dynamics. *Information Fusion*, 41, pp. 255-263.

There may be differences between this version and the published version. You are advised to consult the publisher's version if you wish to cite from it.

<http://eprints.gla.ac.uk/208064/>

Deposited on: 21 January 2020

Enlighten – Research publications by members of the University of Glasgow
<http://eprints.gla.ac.uk>

A fusion framework to estimate plantar ground force distributions and ankle dynamics

Fani Deligianni^a, Charence Wong^a, Benny Lo^a, Guang-Zhong Yang^{a,*}

^a*Hamlyn Centre, Imperial College London, United Kingdom*

Abstract

Gait analysis plays an important role in several conditions, including the rehabilitation of patients with orthopaedic and the monitoring of neurological conditions, mental health problems and the well-being of elderly subjects. It also constitutes an index of good posture and thus it can be used to prevent injuries in athletes and monitor mental health in typical subjects. Usually, accurate gait analysis is based on the measurement of ankle dynamics and ground reaction forces. Therefore, it requires expensive multi-camera systems and pressure sensors, which cannot be easily employed in a free-living environment. We propose a fusion framework that uses an ear worn activity recognition (e-AR) sensor and a single video camera to estimate foot angle during key gait events. To this end we use canonical correlation analysis with a fused-lasso penalty in a two-steps approach that firstly learns a model of the timing distribution of ground reaction forces based on e-AR signal only and subsequently models the eversion/inversion as well as the dorsiflexion of the ankle based on the combined features of e-AR sensor and the video. The results show that incorporating invariant features of angular ankle information from the video recordings improves the estimation of the foot progression angle, substantially.

Keywords: Gait analysis, e-AR, fusion of sensors gait data and video

2010 MSC: 00-01, 99-00

*Corresponding Author

Email address: g.z.yang@imperial.ac.uk (Guang-Zhong Yang)

URL: <http://www.imperial.ac.uk/hamlyn-centre/> (Guang-Zhong Yang)

1. Introduction

Gait analysis is a well-established method for analysing the biomechanics of gait, and a means to capture effective and quantitative assessments for orthopaedic and neurological rehabilitation. Motion capture with topical tracking systems, force plates, instrumented treadmills and pressure sensing insoles are instruments for measuring the heel, subtalar, ankle and knee joint angles, and analysing the force exerted on the ground for accurate analysis of the biomechanical indices of subjects. Although such instrumentations are widely available, the high cost and long set up times typically required have restricted the use of such instruments in major hospitals for routine measurement of certain patients.

Pathological gait is difficult to describe, since it involves atypical ankle kinematics. Nevertheless, it is characterized by the periodic movement of each leg from one position to the next and the corresponding ground reaction forces that support the motion of the body. The ankle is the lower joint and the first to respond to the impact of the foot with the ground. In particular, the subtalar joint, which is lateral to the ankle, is responsible for most of the inversion and eversion of the foot, which plays a significant role in the toe-off phase of the gait as it provides the propulsion to lift the foot. In other words, ground reaction forces along with ankle eversion/inversion and dorsiflexion play a key role in the biomechanical dynamics. Several recent studies have shown that certain gait characteristics can be related to abnormal posture, the development of osteoarthritis and sports related injuries [1, 2, 3, 4, 5]. For example, Kuhman et al. has shown that lower leg and foot dynamics are related to the development of injuries in runners [2]. Furthermore, greater rear-foot pronation has been associated with greater pressure on the medial portions of the plantar surface during walking and it has been observed in individuals with poor postural control [5].

To measure the lower limb kinematics accurately expensive multi-camera configuration systems are used to detect and track reflective skin markers. However, the confined spaces typically available in clinics or at home means these methods cannot easily be applied in these scenarios. The use of monocular vi-

sion has also been proposed for a number of gait analysis applications, such as biometric authentication [6], diagnosis of Parkinson’s disease [7], and identification of abnormalities for assisted living [8, 9]. Some of these works map the 2D extracted trajectories to 3D world coordinate system based on deep neural
35 networks and require several labeled training sets. Furthermore, they assume large distances between the subject and the camera and assumptions that the body mass is planar. This does not allow an accurate estimation of the ankle dynamics and the foot progression angle. Furthermore, estimation of ground reaction forces are also important to determine the health risks over time due
40 to excessive joint loading rates and stress. Accurate measurements of ground reaction forces normally require pressure insoles, which are placed inside the shoes.

Recently, wearable wireless body worn sensors have been proposed for detailed gait analysis [10, 11]. Our previous work has shown the feasibility and
45 accuracy of using the ear-worn activity recognition (e-AR) sensor for detailed gait analysis and activity recognition [12, 13]. This lightweight and miniaturized sensor, e-AR, enables pervasive and continuous monitoring of user with negligible distraction to their normal daily activities. In previous work, we have demonstrated the feasibility of using the e-AR sensor with a hierarchical
50 Bayesian Network framework for estimation of GRFs for normal gait [14]. This hierarchical model allowed characterisation of the plantar force timing distribution based on e-AR measurements only. In a recent article, Clark et al. showed that it is possible to predict vertical ground reaction forces in runners based on the body mass, the contact time between steps and the swing time only [15].
55 [16, 17] compare the advantages of inertial and vision for gait analysis. Although the wearable sensor can estimate the temporal distribution accurately, other detailed gait parameters, such as subtalar joint angle are more difficult to be determined based on inertial sensors only.

In this paper, we propose a novel integrated approach of using the e-AR
60 sensor together with a single video camera, and introduce a framework to fuse the sensing and visual features to reveal the interaction of ground reaction

forces and ankle dynamics during normal and abnormal walking. In particular, we utilize Canonical Correlation Analysis with a fused-lasso penalty (fCCA) to extract features across steps that reveal correlations between the e-AR signal
65 and the timing distribution of key gait events. These events occur when ground reaction forces are maximized in the plantar foot areas, such as heel , mid-foot , front-foot and toes . In a two-steps approach, we use fCCA again to fuse the e-AR signal with features derived from the video analysis of a single camera that reflect an angular interaction between the two legs during walking. In
70 this way, we are able to create a prediction framework of the dorsiflexion and inversion/aversion foot angles during heel, mid-foot, front-foot and toe contacts with the ground.

2. Methods

2.1. Data fusion framework

75 Both normal and pathological gait exhibit repetitive patterns of motion of the lower limbs. In this paper, we utilize this to construct a fusion framework that samples across steps of e-AR signal and video recordings to extract features that predict well ground reaction forces timing distributions and subsequently foot angles in key gait events. Therefore, the framework has two main compo-
80 nents that are constructed independently but they interact to provide detailed gait characteristics. The proposed fusion framework requires time-series derived from e-AR sensor, insole sensors and video features to be segmented into gait steps, independently. This is also important as it alleviate the need for accurate synchronization between different modalities. An overview of the framework is
85 presented in Figure 1.

We are interested in learning a relationship between the e-AR acceleration data and the plantar force timing distributions across steps. The e-AR measures acceleration in three axes that are aligned to the body: Medial-Lateral (ML) axis, Superior-Inferior (SI) axis and Anterior-Posterior (AP) axes. On the other
90 hand, ground reaction forces can be measured with foot pressure insoles that

record the pressure between the planar surface of the foot and the sole of the shoes. In order to estimate the plantar force distributions, we hierarchically subdivide the foot into the Heel, Mid-foot, Front-foot and Toe regions as well as Medial and Lateral regions. This results in eight sub-regions similar to our
95 previous work [14]. The insole data are pre-processed to detect gait steps based on the pressure difference between left and right foot. Subsequently, for each step the timings of the maximums of the sub-plantar force distributions are defined within each region. These timings represent key gait events and they are important in identifying abnormal gait.

Once both insole and e-AR data are segmented into steps, we normalize the e-AR signal at each step with respect to the time axis based on linear interpolation so that all steps are equally sampled. Note that we concatenate horizontally the combined SI and AP signal along with the ML signal. Subsequently, these vectors are concatenated vertically to form a matrix, \mathbf{X} , $m \times 2n$, where m is the number of steps and n is the number of time samples. On the other hand, the response data \mathbf{Y} is a $m \times k$ matrix that reflects the timings of the peaks of the plantar force distribution estimated based on the insole data. k is the number of plantar sub-regions defined. fCCA is used to relate the e-AR waveform data for each step with the GRFs timing distributions obtained from insole data. Canonical correlation analysis is a powerful tool of modelling the correlation between multivariate variables. The projection of \mathbf{X} and \mathbf{Y} on the derived canonical vectors result in maximally linearly correlated variables. Thus, it allows bi-direction predictive modelling of the associated variables and it has been used in high-dimensional spaces of multi-view gait recognition and numerous other applications [18, 19, 20]. fCCA is a variant of canonical correlation analysis that applies a fused lasso penalty, which penalizes the L_1 norm of both the coefficients and their successive differences. This enforces both sparsity and smoothness, which is important since the fCCA variables are time-series segments and ordered variables [21]. The implementation of fCCA is based on a penalized matrix decomposition framework, which obeys the following criterion

[22, 23]:

$$\begin{aligned} & \text{maximise}_{u,v} u^T \mathbf{X}^T \mathbf{Y} v \\ & \text{subject to : } \|u\|^2 \leq 1, \|v\|^2 \leq 1, f_1 \leq c_1, f_2(v) \leq c_2 \end{aligned} \quad (1)$$

Here, f_1, f_2 are convex penalty functions that both impose a fused lasso penalty:

$$f(\mathbf{w}) = \sum_j \|\mathbf{w}_j\| + \sum_j \|\mathbf{w}_j - \mathbf{w}_{j-1}\| \quad (2)$$

100 Note that with u fixed, the criterion in eq. 1 is convex in v , and with v fixed, it is convex in u . Therefore, the objective function of this biconvex criterion increases in each step of an iterative algorithm [23]:

$$\begin{aligned} u & \leftarrow \text{argmax}_u u^T \mathbf{X}^T \mathbf{Y} v \quad \text{subject to : } \|u\|^2 \leq 1, f_1(u) \leq c_1 \\ v & \leftarrow \text{argmax}_v u^T \mathbf{X}^T \mathbf{Y} v \quad \text{subject to : } \|v\|^2 \leq 1, f_2(v) \leq c_2 \end{aligned} \quad (3)$$

Once the fCCA model has been trained it can be used for prediction:

$$\hat{\mathbf{Y}}_s = (u \mathbf{X}_s)^+ \mathbf{D} v^+ \quad (4)$$

Where, \mathbf{D} is the diagonal matrix with the canonical correlation scores and
105 $+$ denotes the pseudo-inverse.

The second major component of the fusion framework is the incorporation of video features derived from a single camera. This provides us with the ability not only to delineate important timing gait events but also estimate the angles between the foot and leg that reflect dorsiflexion and inversion/aversion in these
110 key gait points independently of the camera view point. To this end fCCA is applied again to find a relationship between the combined data derived from e-AR and video features, \mathbf{Z} , and foot angles, \mathbf{W} estimated in key gait events, such as when GRFs are maximized during heel, mid-foot, frontal-foot and toe contacts with the ground. Therefore, \mathbf{Z} is an $m \times 2n$ matrix, where m is the
115 number of steps and n reflects the number of time samples. To form \mathbf{Z} we concatenate horizontally the sum of the AP and SI eAR signal and an index based on cross ratio estimated extracted from single video recordings. \mathbf{W} is a $m \times 2k$ matrix that encodes information about the foot angles (inversion/aversion and

dorsiflexion) in both the left and right foot when the GRFs are maximized in
120 the key foot subregions Heel (H), Mid-foot (M), Front-foot (F) and Toe (T),
Figure 3b. fCCA takes similar form as in equation 1. However, we have replaced
 f_2 fused lasso penalty with a lasso penalty to reflect the fact that \mathbf{W} does not
encode ordered variables.

2.2. Processing of video data

125 To complement the inertial motion data captured using the ear-worn e-AR
sensor, video is used to determine gait features that cannot be obtained through
wearable devices. To capture the characteristics of the subject’s gait from video,
visual tracking and image segmentation steps are performed. Here, we have
recorded the front and back views of the subjects. Our main assumption is that
130 the camera has up-right orientation with respect to the ground.

Tracking. To ensure that the subjects’ gait is evaluated consistently, a state-
of-the-art tracking-by-detection method, kernelized correlation filter (Joao F
Henriques, Caseiro, Martins, Batista, 2012; Joo F Henriques, Caseiro, Martins,
Batista, 2015), is used to locate the lower limbs in each video frame. Histogram
135 of oriented gradients and colour-space features are used to perform multi-scale
tracking of the subject.

Image Segmentation. A clustering algorithm, K-means clustering, is then em-
ployed to segment the tracked region of the image into separate classes of fore-
ground and background. The foreground clusters of interest in this work are
the lower parts of the legs and feet. To improve the robustness of the method
against non-uniform colours in the subject’s footwear, GrabCut [24] is used to
further refine the contours of the segmented body parts. GrabCut is based on
the ‘Graph Cut’ algorithm, which uses a k-Gaussian mixture models to segment
the target object from the background [25]. In an undirected graph, the Graph
Cut aims to find a subset of edges C such that the two terminal nodes are sepa-
rated in the induced graph. The algorithm minimizes an energy cost function \mathbf{E}

that measures how well a colour distribution model h fits the data and imposes smoothness constraints.

$$\mathbf{E}(\alpha, \theta, \mathbf{z}) = \sum_n -\log h(z_n; \alpha_n) + \gamma \sum_{(m,n \in C)} dis(m, n)^{-1} [\alpha_n \neq \alpha_m] \exp -\beta(z_m - z_n)^2 \quad (5)$$

where α is the pixels' label, \mathbf{z} encodes the colour information and θ are the model's parameters. For each pair of neighbour pixels that do not have the same label, the energy function is increased according to the parameter β .

140 Grabcut requires a pre-estimation of a rectangular box or mask that surrounds the feet. We pre-estimate a rectangular area based on the position of the legs and subsequently we refine it iteratively based on the results of GrabCut. Figure 2 shows an example of the contours obtained for the legs and feet as well as the results for lower limb tracking for the four different types of gait
145 considered in this paper.

Contour analysis. Contour analysis on the extracted body parts is then performed to find the orientation of the lower limbs and feet. Localization of individual body parts allows the distances between the left and right foot to be estimated in an invariant way with respect to the distance of the person from the camera. To calculate a view-invariant measure of the lower pose, a cross-ratio between the directions of the legs and feet is used, Fig. 1e):

$$CR = \frac{\cos(L_L, F_L) * \cos(L_R, F_R)}{\cos(L_L, L_L) * \cos(F_R, F_R)} \quad (6)$$

L_L, F_L, L_R, F_R correspond to fitted lines at the left leg, left foot, right leg and right foot, respectively, Figure 2.

2.3. Segmentation of multi-modal time-series data into steps

Both e-AR acceleration data and visual features are segmented into steps based on singular spectrum analysis and peak detection. The preprocessing of e-AR with singular spectrum analysis is based on the acceleration in the SI and AP axis, whereas the segmentation of the visual features is based on the normalized distance between the left and right ankle as it reflected on the

vertical direction of the image plane. Singular spectrum analysis is mainly used to denoise the signal and improve the detection of peaks that reflect foot contacts with the ground [12, 13]. If \mathbf{s} is a time-series, a trajectory matrix is created based on an embedding dimension that reflects the window length of the sub-sampled time-series grouped together:

$$\mathbf{S} = [\mathbf{s}_1, \mathbf{s}_2, \dots, \mathbf{s}_k] = \begin{pmatrix} s_0 & s_1 & \cdots & s_{k-1} \\ s_1 & s_2 & \cdots & s_k \\ \vdots & \vdots & \ddots & \vdots \\ s_{l-1} & s_l & \cdots & s_{n-1} \end{pmatrix} \quad (7)$$

where $k = n - l + 1$, n is the length of the time-series and l is the embedding dimension. This is a Hankel matrix with constant skew-diagonal elements. The singular value decomposition of a Hankel matrix is related to the state-space realization of a Hidden Markov model and it is appropriate for the decomposition of non-stationary signals. The covariance matrix of \mathbf{S} , $\mathbf{C} = \mathbf{S}\mathbf{S}^T$ is decomposed into the eigenvectors \mathbf{u}_i and the corresponding eigenvalues λ_i (Jarchi et al., 2014). Therefore, the trajectory matrix is written as:

$$\mathbf{S} = \mathbf{S}_1 + \mathbf{S}_2 + \cdots + \mathbf{S}_d \quad (8)$$

where $d = \text{argmax}_i\{\lambda_i > 0\}$, $\mathbf{S}_i = \sqrt{\lambda_i}\mathbf{u}_i\mathbf{v}_i^T$ and $\mathbf{v}_i = \mathbf{S}^T\mathbf{u}_i/\sqrt{\lambda_i}$. Finally, the
150 signal is reconstructed based on the diagonal averaging of a subset of the group elementary matrices derived from the decomposition.

3. Results

3.1. Data acquisition

We acquired simultaneous recordings of ear-sensor data and insole data
155 (PAROTEC, Paromed, Germany) from seven healthy volunteers that performed four different styles of walking patterns: normal walking (normal), imitating limping based on unequal time steps (limping), imitating inversion injury (pronation) and imitating eversion injury (supination). For each condition we

recorded four sessions of each subject (total 16 sessions across all conditions)
160 where the subject was asked to walk back and forth in a corridor for a total of
approximately 11 meters. Visual information of each subject’s gait is simulta-
neously captured using a 2D camera with a resolution of 1080p at 30 frames per
second.

3.2. Training and validation

165 Figure 3a shows the average e-AR signal across all subjects and e-AR steps
for normal walking, limping, walking with exaggerate pronation, and walking
with exaggerated supination, respectively. The e-AR signal along IS and AP
and ML axis have been processed based on singular spectrum analysis . Firstly,
singular spectrum analysis is applied in IS, AP and ML axis independently.
170 Subsequently, IS and AP are added together and the singular spectrum analysis
is re-applied. The result is concatenated with the ML e-AR signal to form the
predictive variables X. Here, we note that different styles of walking result in a
phase shift of the e-AR signal when steps are normalized to have the same sample
length. Figure 3b depicts a diagram of the insole sensors that shows how the foot
175 plantar area has been segmented to each region. Firstly, with respect to the AP
axis the foot is segmented to the Toe, Front-foot, Mid-foot and Heel regions.
With respect to the ML axis, the foot is segmented to Medial and Lateral
regions. Subsequently, sub-regions are defined as Heel-Lateral, Heel-Medial,
Midfoot-Lateral, Midfoot-Medial, Front-foot-Lateral, Front-foot-Medial, Toe-
180 Lateral, Toe-Medial. The predictive/response variables Y are shown in Figure
4. This shows the plantar GRFs timing distributions across all subjects for each
condition. Gait events have been identified based on insole data and they have
been normalized with respect to each insole step. Gait events have been sorted
based on their mean value during normal walking.

185 Due to the difference in shoe size, foot pressure insoles are expensive. With
the aim of providing a low cost approach for gait analysis, we are interested in
devising a model that encodes the relationship between e-AR and insole data.
Furthermore, we would like to be able to get accurate measurements of the

events timing in abnormal walking patterns. Therefore, we train and test our
190 model based on leave-one-out cross validation in the following scenarios:

- Within subjects and within conditions: To form the training dataset, the data across three sessions are concatenated in each walking condition/pattern and each subject independently. The fourth session is used for testing. The mean errors and mean standard deviations are averaged
195 across subjects and cross-validation rounds.
- Across subjects and within conditions: To form the training dataset, the data across all subjects and within each condition are concatenated. Subsequently, leave-one-out cross validation is used to estimate the mean error and mean standard deviation, Figure 5a.
- 200 • Across subjects and across conditions: Data across subjects and across conditions are concatenated and leave-one-out cross validation is used to estimate the mean error and mean standard deviation, Figure 5b.

We note a significant error reduction when we train the model across subjects and conditions. The results show that training the fCCA model with data
205 acquired with normal walking as well as pathological variations enhances the prediction performance. Perhaps, this reflects that the model is more robust to outliers. Outliers can originate from both false positive and false negative detection of foot contacts with the ground. The results also show that the identification of heel contact is relatively the most accurate across all conditions and
210 training scenarios. This is expected since heel contacts in normal walking is the first foot contact with the ground and therefore the change in the acceleration is rapid.

In order to evaluate the proposed measure of angular variation based on a cross ratio, CR, we estimate the correlation between several extracted video
215 features and the normalized distance between left and right ankle in the vertical direction of the image plane. Figure 6a shows an example of the extracted features from the analysis of the video when the subject walk towards the camera.

These features include the dot products between the two legs , the two feet ,
the right leg and right foot and the left leg and left foot . Figure 6b shows that
220 CR correlates well to the normalised distance between left and right ankle in
the vertical direction of the image plane across all subjects and conditions.

In Figure 7, we demonstrate the performance of fCCA in fusing the e-AR
signal with the derived video features, namely CR, to model the foot angle
progression. Figure 7a show the error in radians based on leave-one-out cross
225 validation of the proposed method. The fCCA model estimates the dorsiflexion
and the aversion /inversion of the ankle when ground reaction forces at
the heel , mid-foot , front-foot and toes are maximized. Therefore, we show
the mean errors and standard deviation of estimating DF and EI at Heel, Mid-
foot, Front-foot and Toes contact with the ground. Note that the results from
230 left/right foot have been averaged accordingly. Ground truth data have been
measured based on the identification of the knee, ankle and toes manually in
each frame and subsequently estimating dorsiflexion as the angle of the foot
with the vertical image plane axis and inversion/eversion as the angle of the
foot with the horizontal image plane axis. Figure 7b-7e shows the difference of
235 angular error between a model that uses only e-AR to predict foot angle pro-
gression and the proposed method for each of the conditions: normal walking,
limping, pronation and supination, respectively. Although, we show the results
summarized independently in each condition, the fCCA model has been trained
based on cross-validation across all conditions at once. The proposed fusion
240 method outperforms the model based on e-AR data only in most of the cases
by a significant level. In fact, using the e-AR approach to estimate foot angle
information during limping is inaccurate, possibly, due to the asymmetry be-
tween right and left gait steps. Nevertheless, combining e-AR signal and video
features improves the performance in most other walking patterns too. The re-
245 duction in the performance of the proposed method during pronation may result
from inaccuracies in segmenting the video features into steps. This could reflect
the fact that the vertical distance between the right and left ankle is smaller in
pronation.

4. Discussion

250 A number of approaches based on inertial sensors, cameras and computer
vision algorithms have been proposed to measure gait characteristics, such as
step length, foot angles and ground reaction forces. Most of them are based
on system configurations that are difficult to be installed in a free-living en-
255 vironment. For example, these systems involve installing markers on the floor
and or on the shoe [26]. On the other hand, advanced gait recognition systems
use inertial sensors to assess gait as a biometric trait for security/surveillance
applications [27, 28]. These systems are useful to identify individuals based on
their gait characteristics but analysing gait for clinical assessment requires un-
260 derstanding the dynamics of the joint loading rates and stress, which are directly
related to ground reaction forces and angles between the lower limb segments.
These measurements are used to provide objective and reliable estimates of the
progression of diseases in neurological conditions, stroke rehabilitation, ageing
and orthopaedics [29].

The proposed framework exploits fCCA in a two-steps approach. Firstly,
265 fCCA is used to extract the coefficients that relate the e-AR signal across steps
to the timing distribution of ground reaction forces estimated based on insole
sensors data. To verify that the proposed model is generalizable to new subjects,
leave-one-out cross validation is used on the concatenated training sets across
subjects and conditions. Subsequently, we use fCCA again to fuse the e-AR sig-
270 nal with visual features that reflect angular information of the lower limbs. This
model learns a relationship between the fused information and the foot angle at
key gait events, which reflect maximum ground reaction forces at heel, mid-foot,
front-foot and toes, respectively. fCCA is based on a penalized decomposition
method that imposes a fused lasso penalty on the coefficients that results in
275 smoothness. We adapted this method because it can handle high dimensional
data and it takes into account that the fCCA variables are ordered/time-series
data. The extracted coefficients are sparse and they can reveal further which
variables play a critical role in the prediction. Other approaches like deep neural

networks may be an interesting alternative of fusing information across different
280 sensors and/or video. However, they require an abundance of training datasets
that include insole recordings and angle measurements across patients groups.

Our method requires that both the e-AR signal and the extracted visual fea-
tures are segmented into steps. There are several advantages with this approach.
Firstly, the model is less sensitive to over-fitting even with a small number of sub-
285 jects, since training samples are across steps. Furthermore, it does not require
accurate synchronization between the multi-modal signals. However, the accu-
racy of the approach depends on the segmentation of multivariate time-series
data, which is not a trivial problem and in abstract biological applications it
involves high computational complexity [30]. Our previous work has shown that
290 based on singular spectrum analysis, the e-AR signal can be reliably processed
in a fraction of a second to derive clinically relevant gait parameters such as
timing of initial foot contact, step time, swing time and stance time [12, 13].
Here, we have used singular spectrum analysis and peak detection to segment
both the e-AR signal and the signal derived from the analysis of the video.

295 It is worth noting that our framework only requires to match steps across
modalities, which is a significant simplification of the synchronisation problem
[31, 32]. Steps are detected independently in each modality based on peak
detection that correspond to initial foot contacts with the ground. For example,
the peaks of the e-AR signal normally correspond to the initial foot contacts
300 and they also correspond to the peaks of the ground reaction forces reflected
in the insole data. The video data was processed to extract the normalised
distance between left and right ankle in the vertical direction of the image plane
and the cross-ratio. All these signals are periodic in nature with peaks that
reflect left and right foot contact. However, the performance of the proposed
305 algorithm would be affected when peaks are not consistently detected within
each modality. In our approach is not important whether the peaks reflect
exactly the same gait event across modalities. Furthermore, a large portion of
errors in peak detection can be identified and filtered out based on the step time
duration.

310 For the analysis of the video state-of-the art tracking technology is used and
combined with advanced image segmentation approaches to identify the lower
limb parts. Tracking of each limb segment independently is challenging even
under controlled conditions. For this reason, we used tracking just to identify
the area of legs and subsequently we utilize image segmentation approaches to
315 segment background from foreground pixels. Subsequently, we applied Grabcut
iteratively to segment the area of foot. Our results are promising and they can
correctly segment the feet even when the subject is at the far end of the corridor.

To our knowledge there is very little work on gait analysis based on a single
RGB camera. Accurate estimation of the angles between lower limbs, such as
320 dorsiflexion and inversion/aversion angles based on marker-less motion capture
is discussed by Sandau et al. [33]. In clinical settings, lower limbs angle es-
timation requires a laboratory environment for the placement of markers and
multi-camera tracking, which is the gold standards for gait analysis. Marker-less
systems have been developed but they also require multi-camera setup and even
325 then, their accuracy is significantly compromised [33]. RGB-D sensors are able
to acquire much more information on the scene with just one infrared camera.
Out-of-the-box algorithms that come with devices such as Kinect extract the
joints of the whole human body in real time. However, there is considerable
jitter on the measured 3D location of the joints and their accuracy depends on
330 the view angle. These factors compromise the use of these devices in estimating
accurate angular measurements in clinical scenarios [34, 35, 36]. In fact, hip
and knee angle correlations between estimated and multi-camera ground-truth
data were lower than 0.3 and 0.8, respectively[34]. To deal with these problems
Ye et al. [36]used markers and an RGB-D system to extract gait character-
335 istics. Nevertheless, the error in the knee angle estimation can get up to 10
degrees during key gait events. Sundau et al. [33]used a marker-less motion
capture system based on eight cameras to recover the joint angles with average
accuracy of -0.7 ± 1.8 and 0.5 ± 2.9 degrees for dorsal/plantar flexion and ev-
ersion/inversion, respectively. However, the mean error in key gait events can
340 go up to -1.0 ± 2.7 and 3.9 ± 2.8 degrees for dorsal/plantar flexion and ever-

sion/inversion, respectively. Our results based only on one camera and the e-AR sensor compare well with dorsal/plantar flexion average error around 4.5 ± 2.43 degrees and eversion-inversion mean error 2.29 ± 1.14 degrees at heel strike.

Our results show that the accuracy of the estimated ankle angle is affected by the walking pattern. For example, dorsal/plantar flexion and eversion/inversion have been identified more accurately during normal walking and pronation compared to limping and supination. The reason for this is that step identification is harder during limping and supination. It should be noted that step identification is independent in each modality. Nevertheless, our approach can be extended to minimise errors during asymmetric gait such as limping by explicitly accounting for left and right steps in the training procedure of the fCCA model. Another limitation is that we have identified 2D angles as opposed to 3D angles. To alleviate this issue we suggested a novel measure based on the cross-ratio between the foot and the leg, which is relatively invariant to the camera view. However, this measure is not yet adopted to clinical scenario and it more difficult to be interpreted. Finally, our method uses GrabCut and clustering approaches to segment the foot and leg. Therefore, its success depends on the contrast between foreground and background pixels.

We asked healthy volunteers to walk normally as well as to imitate limping, pronation and supination. Therefore, our population variance and motion of the lower limbs may not represent accurately the variance observed in real pathological cases. We have used leave-one-out cross validation to determine the out-of-sample mean modelling error and standard deviation. The error is statistically significant in all cases. However, further work that would involve validation based on multi-camera tracking and confidence interval estimation is required for patient cohorts.

5. Acknowledgements

We would like to thank Dr. Daniele Ravi and acknowledge EPSRC as the funding body for this study: Smart Sensing for Surgery (EP/L014149/1).

370 **References**

- [1] D. A. Bruening, T. E. Cooney, M. S. Ray, G. A. Daut, K. M. Cooney, S. M. Galey, Multisegment foot kinematic and kinetic compensations in level and uphill walking following tibiotalar arthrodesis, *Foot and Ankle International* 37 (10) (2016) 1119–1129. doi:10.1177/1071100716655205.
375 URL <GotoISI>://WOS:000385345300013
- [2] D. J. Kuhman, M. R. Paquette, S. A. Peel, D. A. Melcher, Comparison of ankle kinematics and ground reaction forces between prospectively injured and uninjured collegiate cross country runners, *Human Movement Science* 47 (2016) 9–15. doi:10.1016/j.humov.2016.01.013.
380 URL <GotoISI>://WOS:000375167500002
- [3] R. A. Resende, R. N. Kirkwood, K. J. Deluzio, E. A. Hassan, S. T. Fonseca, Ipsilateral and contralateral foot pronation affect lower limb and trunk biomechanics of individuals with knee osteoarthritis during gait, *Clinical Biomechanics* 34 (2016) 30–37. doi:10.1016/j.clinbiomech.2016.03.005.
385 URL <GotoISI>://WOS:000375808800006
- [4] K. E. Roach, B. B. Wang, A. L. Kapron, N. M. Fiorentino, C. L. Saltzman, K. B. Foreman, A. E. Anderson, In vivo kinematics of the tibiotalar and subtalar joints in asymptomatic subjects: A high-speed dual fluoroscopy study, *Journal of Biomechanical Engineering-Transactions of the Asme* 138 (9). doi:Artn09100610.1115/1.4034263.
390 URL <GotoISI>://WOS:000383260200006
- [5] D. D. Silva, F. H. Magalhaes, M. F. Pazzinatto, R. V. Briani, A. S. Ferreira, F. A. Aragao, F. M. de Azevedo, Contribution of altered hip, knee and foot kinematics to dynamic postural impairments in females with patellofemoral pain during stair ascent, *Knee* 23 (3) (2016) 376–381. doi:10.1016/j.knee.2016.01.014.
395 URL <GotoISI>://WOS:000378963600007

- [6] G. Rogez, J. Rihan, J. J. Guerrero, C. Orrite, Monocular 3-d gait tracking
400 in surveillance scenes, *Ieee Transactions on Cybernetics* 44 (6) (2014) 894–
909.
URL <GotoISI>://WOS:000337960000014
- [7] C. W. Cho, W. H. Chao, S. H. Lin, Y. Y. Chen, A vision-based analysis
405 system for gait recognition in patients with parkinson’s disease, *Expert
Systems with Applications* 36 (3) (2009) 7033–7039.
URL <GotoISI>://WOS:000263817100156
- [8] M. Nieto-Hidalgo, F. J. Ferrandez-Pastor, R. J. Valdivieso-Sarabia,
J. Mora-Pascual, J. M. Garcia-Chamizo, A vision based proposal for classi-
410 fication of normal and abnormal gait using rgb camera, *Journal of Biomed-
ical Informatics* 63 (2016) 82–89.
URL <GotoISI>://WOS:000389557000009
- [9] E. E. Stone, M. Skubic, Passive in-home measurement of stride-to-stride
gait variability comparing vision and kinect sensing, 2011 Annual Interna-
415 tional Conference of the Ieee Engineering in Medicine and Biology Society
(Embc) (2011) 6491–6494.
URL <GotoISI>://WOS:000298810005008
- [10] C. Wong, Z. Q. Zhang, B. Lo, G. Z. Yang, Wearable sensing for solid
biomechanics: A review, *Ieee Sensors Journal* 15 (5) (2015) 2747–2760.
doi:10.1109/Jsen.2015.2393883.
420 URL <GotoISI>://WOS:000352624500006
- [11] N. Raveendranathan, S. Galzarano, V. Loseu, R. Gravina, R. Giannan-
tonio, M. Sgroi, R. Jafari, G. Fortino, From modeling to implementation
of virtual sensors in body sensor networks, *IEEE Sensors Journal* 12 (3)
(2012) 583–593. doi:10.1109/JSEN.2011.2121059.
- 425 [12] D. Jarchi, C. Wong, R. M. Kwasnicki, B. Heller, G. A. Tew, G. Z.
Yang, Gait parameter estimation from a miniaturized ear-worn sensor

using singular spectrum analysis and longest common subsequence, *Ieee Transactions on Biomedical Engineering* 61 (4) (2014) 1261–1273. doi:10.1109/Tbme.2014.2299772.

430 URL <GotoISI>://WOS:000337739300024

- [13] D. Jarchi, B. Lo, C. Wong, E. Jeong, D. Nathwani, G. Z. Yang, Gait analysis from a single ear-worn sensor: Reliability and clinical evaluation for orthopaedic patients, *Ieee Transactions on Neural Systems and Rehabilitation Engineering* 24 (8) (2016) 882–892. doi:10.1109/Tnsre.2015.2477720.

435 URL <GotoISI>://WOS:000381496500007

- [14] B. Lo, J. Pansiot, G. Z. Yang, Bayesian analysis of sub-plantar ground reaction force with bsn, *Sixth International Workshop on Wearable and Implantable Body Sensor Networks, Proceedings* (2009) 133–137doi:10.1109/P3644.37.

440 URL <GotoISI>://WOS:000275810500023

- [15] K. P. Clark, L. J. Ryan, P. G. Weyand, A general relationship links gait mechanics and running ground reaction forces, *Journal of Experimental Biology* 220 (2) (2017) 247–258. doi:10.1242/jeb.138057.

URL <GotoISI>://WOS:000392154200018

- 445 [16] I. H. Lpez-Nava, I. Gonzlez, A. Muoz-Melndez, J. Bravo, Comparison of a Vision-Based System and a Wearable Inertial-Based System for a Quantitative Analysis and Calculation of Spatio-Temporal Parameters, Springer International Publishing, Cham, 2015, pp. 116–122. doi:10.1007/978-3-319-26508-7_12.

450 URL http://dx.doi.org/10.1007/978-3-319-26508-7_12

- [17] I. Gonzalez, I. H. Lopez-Nava, J. Fontecha, A. Munoz-Melendez, A. I. Perez-SanPablo, I. Quinones-Uriostegui, Comparison between passive vision-based system and a wearable inertial-based system for estimating temporal gait parameters related to the gaitrite electronic walkway, *Jour-*

- 455 nal of Biomedical Informatics 62 (2016) 210–223.
URL <GotoISI>://WOS:000384703800020
- [18] F. Deligianni, M. Centeno, D. W. Carmichael, J. D. Clayden, Relating
resting-state fmri and eeg whole-brain connectomes across frequency bands,
Frontiers in Neuroscience 8. doi:ARTN25810.3389/fnins.2014.00258.
460 URL <GotoISI>://WOS:000346512300001
- [19] F. Deligianni, D. W. Carmichael, G. H. Zhang, C. A. Clark, J. D. Clayden,
Noddi and tensor-based microstructural indices as predictors of functional
connectivity, Plos One 11 (4). doi:ARTNe015340410.1371/journal.pone.
0153404.
465 URL <GotoISI>://WOS:000374131700051
- [20] X. L. Xing, K. J. Wang, T. Yan, Z. W. Lv, Complete canonical correlation
analysis with application to multi-view gait recognition, Pattern Recognition
50 (2016) 107–117. doi:10.1016/j.patcog.2015.08.011.
URL <GotoISI>://WOS:000364893700008
- 470 [21] R. Tibshirani, M. Saunders, S. Rosset, J. Zhu, K. Knight, Sparsity and
smoothness via the fused lasso, Journal of the Royal Statistical Society
Series B-Statistical Methodology 67 (2005) 91–108.
URL <GotoISI>://WOS:000225686900006
- [22] D. M. Witten, R. Tibshirani, T. Hastie, A penalized matrix decomposition,
475 with applications to sparse principal components and canonical correlation
analysis, Biostatistics 10 (3) (2009) 515–534.
URL <GotoISI>://WOS:000267213700010
- [23] D. M. Witten, R. J. Tibshirani, Extensions of sparse canonical correlation
analysis with applications to genomic data, Statistical Applications in Ge-
480 netics and Molecular Biology 8 (1).
URL <GotoISI>://WOS:000267601500008

- [24] C. Rother, V. Kolmogorov, A. Blake, "grabcut": interactive foreground extraction using iterated graph cuts, *ACM Trans. Graph.* 23 (3) (2004) 309–314. doi:10.1145/1015706.1015720.
- 485 [25] Y. Y. Boykov, M. P. Jolly, Interactive graph cuts for optimal boundary and region segmentation of objects in n-d images, Eighth IEEE International Conference on Computer Vision, Vol I, Proceedings (2001) 105–112.
URL <GotoISI>://WOS:000170817100014
- [26] T. N. Do, Y. S. Suh, Gait analysis using floor markers and inertial sensors, *Sensors* 12 (2) (2012) 1594–1611. doi:10.3390/s120201594.
490 URL <GotoISI>://WOS:000300720300025
- [27] G. Panahandeh, N. Mohammadiha, A. Leijon, P. Handel, Continuous hidden markov model for pedestrian activity classification and gait analysis, *Ieee Transactions on Instrumentation and Measurement* 62 (5) (2013) 1073–
495 1083. doi:10.1109/Tim.2012.2236792.
URL <GotoISI>://WOS:000317361500023
- [28] S. Sprager, M. B. Juric, Inertial sensor-based gait recognition: A review, *Sensors* 15 (9) (2015) 22089–22127. doi:10.3390/s150922089.
URL <GotoISI>://WOS:000362512200056
- 500 [29] A. Muro-de-la Herran, B. Garcia-Zapirain, A. Mendez-Zorrilla, Gait analysis methods: An overview of wearable and non-wearable systems, highlighting clinical applications, *Sensors* 14 (2) (2014) 3362–3394. doi:10.3390/s140203362.
URL <GotoISI>://WOS:000335887900072
- 505 [30] N. Omranian, B. Mueller-Roeber, Z. Nikoloski, Segmentation of biological multivariate time-series data, *Scientific Reports* 5. doi:ARTN893710.1038/srep08937.
URL <GotoISI>://WOS:000351137000005

- [31] G. Fortino, R. Giannantonio, R. Gravina, P. Kuryloski, R. Jafari, Enabling
510 effective programming and flexible management of efficient body sensor net-
work applications, *IEEE Transactions on Human-Machine Systems* 43 (1)
(2013) 115–133. doi:10.1109/TSMCC.2012.2215852.
- [32] R. Gravina, P. Alinia, H. Ghasemzadeh, G. Fortino, Multi-sensor
fusion in body sensor networks: State-of-the-art and research
515 challenges, *Information Fusion* 35 (2017) 68 – 80. doi:https:
//doi.org/10.1016/j.inffus.2016.09.005.
URL [http://www.sciencedirect.com/science/article/pii/
S156625351630077X](http://www.sciencedirect.com/science/article/pii/S156625351630077X)
- [33] M. Sandau, H. Koblauch, T. B. Moeslund, H. Aanaes, T. Alk-
520 jaer, E. B. Simonsen, Markerless motion capture can provide re-
liable 3d gait kinematics in the sagittal and frontal plane, *Medi-
cal Engineering and Physics* 36 (9) (2014) 1168–1175. doi:http:
//dx.doi.org/10.1016/j.medengphy.2014.07.007.
URL [http://www.sciencedirect.com/science/article/pii/
S1350453314001775](http://www.sciencedirect.com/science/article/pii/S1350453314001775)
- [34] E. Auvinet, F. Multon, J. Meunier, New lower-limb gait asymmetry indices
based on a depth camera, *Sensors* 15 (3) (2015) 4605–4623. doi:10.3390/
s150304605.
URL <http://www.mdpi.com/1424-8220/15/3/4605>
- [35] B. Muller, W. Ilg, M. A. Giese, N. Ludolph, Validation of enhanced kinect
530 sensor based motion capturing for gait assessment, *PLOS ONE* 12 (4)
(2017) 1–18. doi:10.1371/journal.pone.0175813.
URL <https://doi.org/10.1371/journal.pone.0175813>
- [36] M. Ye, C. Yang, V. Stankovic, L. Stankovic, A. Kerr, A depth camera mo-
535 tion analysis framework for tele-rehabilitation: Motion capture and person-
centric kinematics analysis, *IEEE Journal of Selected Topics in Signal Pro-
cessing* 10 (5) (2016) 877–887. doi:10.1109/JSTSP.2016.2559446.

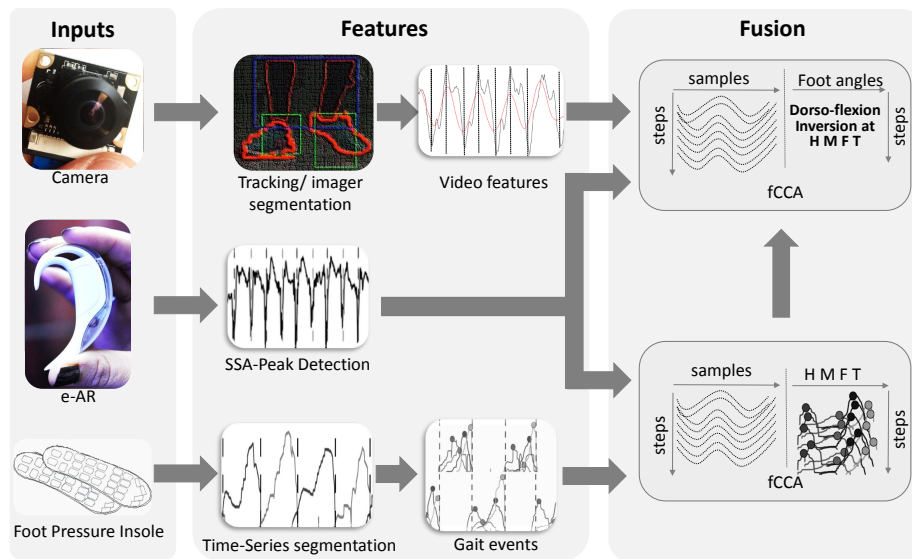


Figure 1. Data fusion framework for gait analysis. fCCA is used in a two steps approach to firstly model the timing distribution of GRFs that reflect key gait events such as when GRFs are maximized in plantar foot areas, such as the heel (H), midfoot (M), frontfoot (F) and toes (T). Subsequently, angular features derived from video tracking and image segmentation approaches are incorporated in another fCCA framework to model foot progression angle during these key gait events.

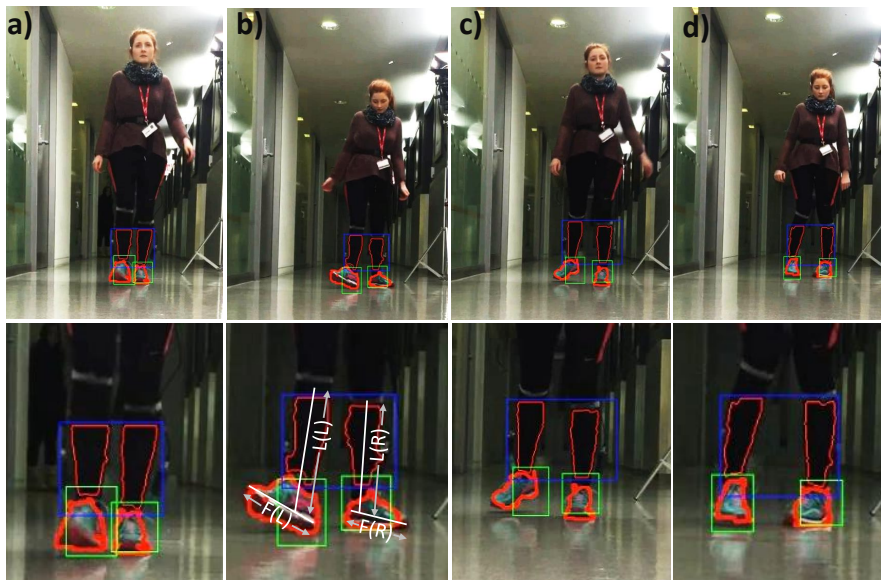
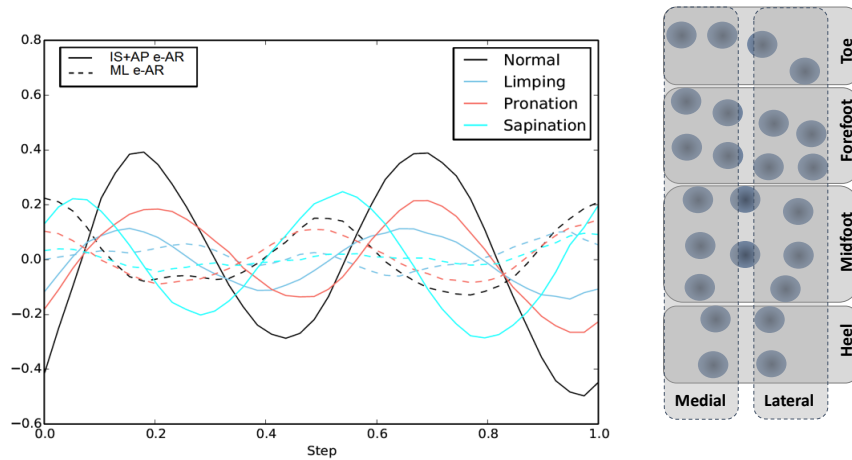


Figure 2. Examples of the lower limb visual tracking (blue), predicted foot regions (green), and leg and foot contours (red) obtained using K-means clustering and GrabCut are shown for the four types of gait considered in this paper; (a) normal, (b) supination, (c) limping and (d) pronation. A diagram of the fitted lines estimated based on image segmentation of the lower limbs has been overlaid on b) .



(a) e-AR training data

(b) plantar foot subregions

Figure 3. a) Average e-AR signal across all subjects for normal walking, limping, walking with exaggerate pronation, and walking with exaggerated supination, respectively. The solid lines represent the summation of the e-AR signal along IS and AP after applying singular spectrum analysis . The dashed lines represent the e-AR signal in ML axis after the application of singular spectrum analysis. b) Plantar foot area subdivision into total eight areas. The plantar foot area is firstly subdivided into four regions across the antero-posterior axis, namely Heel, Midffot, Frontfoot and Toes and in two regions across the medial-lateral axis, namely, Medial and Lateral.

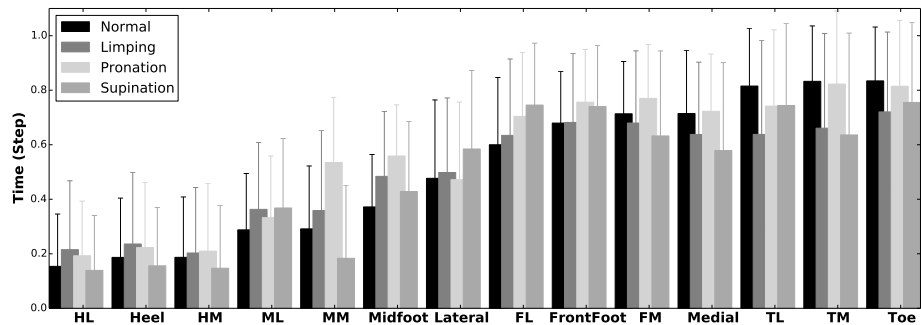
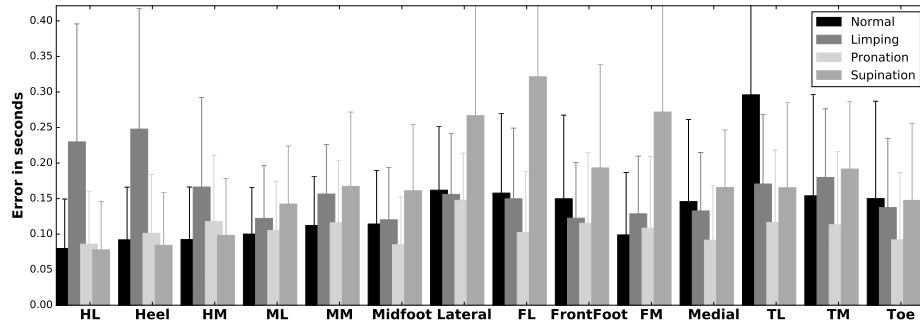
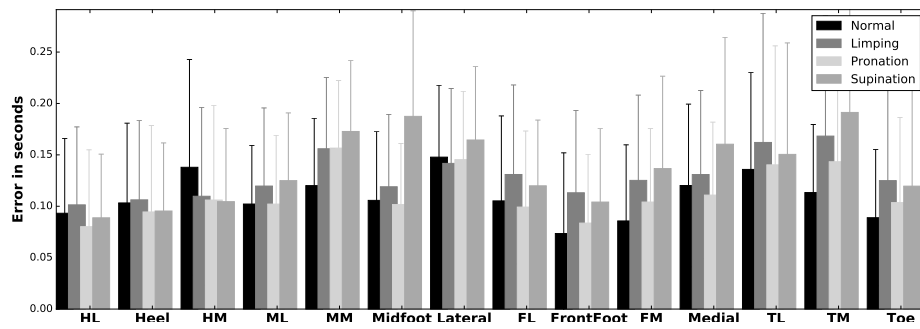


Figure 4. Plantar ground reaction forces timing distributions across all subjects for each conditions. Gait events have been identified based on insole data and they have been normalized with respect to each insole step.

Sub-regions are defined as Heel-Lateral (HL), Heel-Medial (HM), Midfoot-Lateral (ML), Midfoot-Medial (MM), Frontfoot-Lateral (FL), FrontFoot-Medial (FM), Toe-Lateral (TL), Toe-Medial (TM) based on the subdivision of the plantar foot area shown in Figure 3b.



(a) Across subjects and within conditions



(b) Across subjects and across conditions

Figure 5. Leave-on-out cross validation results of the fCCA model in predicting the ground reaction forces timing distributions. a) Across subjects and within conditions: To form the training dataset, the data across all subjects and within each condition are concatenated. b) Across subjects and across conditions: Data across subjects and across conditions are concatenated.

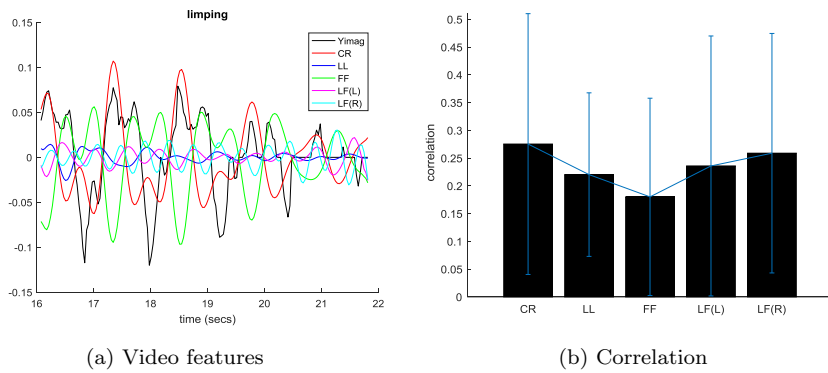
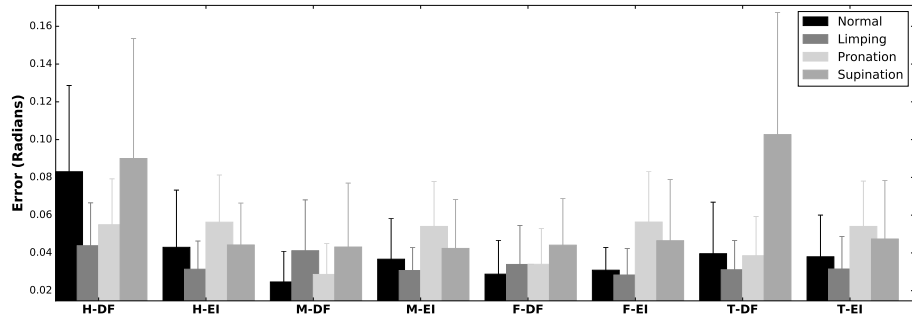
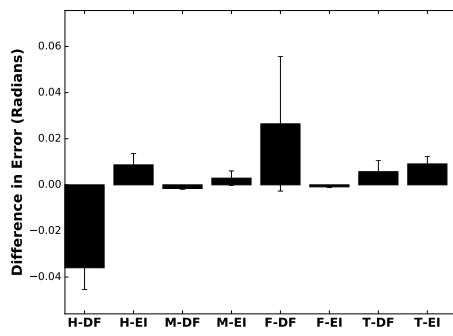


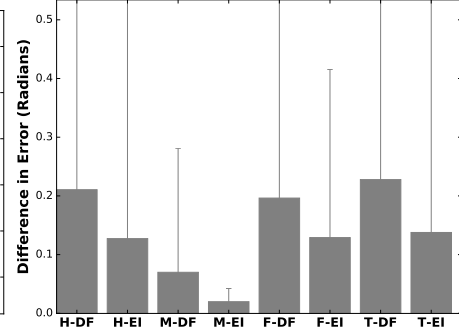
Figure 6. a) An example of the extracted features from the analysis of the video when the subject walks towards the camera. Yimag is the scale invariant distance in the vertical direction of the image plane between left and right ankle. LL is the dot product between the two legs, FF is the dot product between the feet, LF(R) is the dot product between the right leg and right foot and LF(L) is the dot product between the left leg and left foot. b) Absolute correlation values between Yimag, which reflects the distance between right and left feet, and the CR, LL, FF, LF(L) and LF(R), respectively.



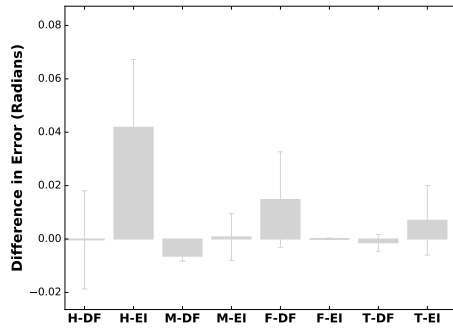
(a) e-AR & Visual Features prediction performance



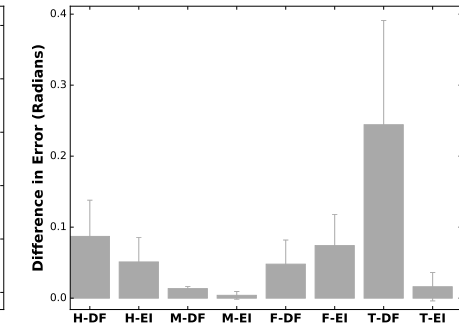
(b) Normal



(c) Limping



(d) Pronation



(e) Supination

Figure 7. The performance of fCCA in fusing the e-AR signal with the derived video features, namely CR, to model the foot angle progression. a) Error in radians based on leave-one-out cross validation of the proposed method. The fCCA model estimates the dorsiflexion (DF) and the aversion /inversion (EI) of the ankle when ground reaction forces at the Heel (H), Mid-foot (M), Front-foot (F) and Toes (T) are maximized. Therefore, we show the mean errors and standard deviation of estimating DF and EI at Heel, Mid-foot, Front-foot and Toes contact with the ground as H-DF, H-EI, M-DF, M-EI, F-DF, F-EI, T-DF, T-EI, respectively. b-e) Differences of angular error between a model that uses only e-AR to predict foot angle progression and the proposed method.